International Journal of Engineering Science 59 (2012) 140–155

Contents lists available at SciVerse ScienceDirect

International Journal of Engineering Science

journal homepage: www.elsevier.com/locate/ijengsci

On certain problems of deformation-induced material instabilities

D. Walgraef [a,1], E.C. Aifantis [a,b,c,*]

[a] Laboratory of Mechanics and Materials, Aristotle University of Thessaloniki, 54124 Thessaloniki, Greece
[b] Michigan Technological University, Houghton, MI 49931, USA
[c] King Abdulaziz University, 21589 Jeddah, Saudi Arabia

ARTICLE INFO

Article history:
Received 12 April 2011
Received in revised form 3 November 2011
Accepted 21 November 2012
Available online 28 April 2012

Keywords:
Material instabilities
Dislocation patterning
Shear banding
Heteroepitaxial film growth

ABSTRACT

Deformation-induced material instabilities may be of elastic (buckling, martensitic transformations) or plastic (necking/shear banding, dislocation patterning) type. In plasticity, the emergence of material instabilities is mainly associated with the properties of the underlying microstructure such as the motion, interaction and production/annihilation of dislocations: the carriers of plastic deformation. In any case, a common mathematical basis for describing the emergence and evolution of pattern-forming material instabilities in a large class of physical problems may be sought on non-monotonous equations of state, in conjunction with the introduction of suitable time and space derivatives in the state variables. This was an approach elaborated upon by Aifantis and co-workers in the early eighties for plastic instabilities. In about the same time, a similar and perhaps broader approach, based on a non-convex energy functional for various physical systems and the introduction of higher-order field variables to stabilize the behavior in the non-convex regime, was independently proposed by Berdichevsky and co-workers. This paper, written on the occasion of his 65th birthday, provides an updated discussion of dislocation patterning, shear banding and strain instabilities during epitaxial film growth.

1. Introduction

The term "Material Instabilities" was introduced as the title of a Special Issue of Res Mechanica (Aifantis, Walgraef, & Zbib, 1988) edited by the authors and H.M. Zbib (then a doctoral student of ECA). The special issue featured articles by Coleman, Vardoulakis, Ghoniem, Neuhauser, Estrin/Kubin, Zbib/Aifantis and Walgraef/Aifantis; partly in response to a proposal advanced a few years earlier by Aifantis (1984) who introduced higher order gradients of internal variables in non-convex (non-monotonous) constitutive equations for capturing the occurrence and evolution of deformation-induced material instabilities (dislocation patterns, shear bands, traveling strain fronts). Even though, in general, a rich physical problem has its specific features that need to be discovered and analyzed for its own merits (e.g. turbulence does not fit in the present framework in an obvious way), the proposed procedure may be viewed as a first step towards a qualitative (and some times quantitative) understanding of the pattern-forming instabilities involved. Dislocation dynamics is exactly such a subject (in a certain sense, it may be viewed as the "turbulence" of solid mechanics, even though the resulting dislocation structures are metastable as being characterized by much larger, as compared to fluids, relaxation times) and there is more to it than fitting into some a priori general recipe. For example, recent work has shown that a proper extension of the classical theory of continuously distributed dislocations leads to degenerate parabolic systems of equations which show richer equilibria than Cahn–Hilliard type of equations. The associated dynamical behavior seems to be describable by hyperbolic systems of

* Corresponding author.
E-mail address: mom@mom.gen.auth.gr (E.C. Aifantis).
[1] Former affiliation: Center for Nonlinear Phenomena and Complex Systems, Universite Libre de Bruxelles, GP 231, B-1050 Bruselles, Belgium.

0020-7225/$ - see front matter © 2012 Published by Elsevier Ltd.
http://dx.doi.org/10.1016/j.ijengsci.2012.03.017

conservation laws without the drawback of ambiguous shocks; and thus, with little doubt, capable of producing microstructures. Moreover, the theory of continuously distributed dislocations is kinematically rigorous (unlike what is proposed here where kinematics is not explicitly considered) and has a history that predates the authors' reaction–transport–diffusion (RTD) approach. More comments on recent efforts to render such an elegant previously existing framework into a workable theory for dislocation patterning are provided in the last section of this article.

Until the publication of the above mentioned article (Aifantis, 1984), there was no convincing theory to address such type of plastic instability problems associated with material softening (negative slope regime in the stress–strain curve, or non-convexity in corresponding equations of state). Even after the publication of Aifantis (1984), several authors insisted-often with unsuccessful attempts-upon regularizing the "homogeneous unstable" material behavior in the softening regime through viscous terms or other artificial means, until it became obvious that higher order gradients are necessary to address spatio–temporal instabilities in dislocation dynamics and plasticity theory, as was the case for other far-from-thermodynamic-equilibrium driven systems.

In the case of dislocation patterning, in particular, an initial reaction–transport–diffusion (RTD) model, commonly known today as the Walgraef–Aifantis (W–A) model (Pontes, Walgraef, & Aifantis, 2006; Walgraef & Aifantis, 1985a, 1985b) was the main motivation for the voluminous subsequent work on discrete dislocation dynamics (DDD) simulations (Ghoniem, Busso, Kioussis, & Huang, 2003; Kubin et al., 1993; Rhee, Zbib, Hirth, Huang, & de la Rubia, 1998), as well as more recent work on density-based statistical dislocation considerations (El-Azab, 2000; Groma, 1997; Zaiser, Miguel, & Groma, 2001). In the case of shear banding and traveling strain fronts, Aifantis' initial gradient plasticity model (Aifantis, 1984, 1987) has served as basis for incorporating higher order gradients to soil plasticity and damage theories, for eliminating mesh-size dependence in finite element computations, as well as for interpreting size effects observed in micro/nano composite materials and recorded during micro/nano indentation (Aifantis & Willis, 2005; Fleck, Muller, Ashby, & Hutchinson, 1994; Gurtin & Anand, 2009; Vardoulakis & Aifantis, 1989).

In parallel with (and independently from) the aforementioned research activity, Berdichevskii and Truskinovskii (1985) presented a similar generic discussion on various types of instabilities occurring in physical systems with localized energy (elementary particles, vapor bubbles in a liquid, dimples in shells, dislocations in crystals, etc). The approach was again based on assuming that the free energy of the system is the sum of two terms: one being a non-convex functional of the field variables and the other being a quadratic functional of their gradients. Even earlier than that, Berdichevskii and Sedov (1967) have presented a dynamic theory of continuously distributed dislocations where the internal energy and the dissipation potential depended on both plastic strain gradients and plastic rotation gradients, which appeared only in special combinations in the form of the dislocation density tensor.

As is often the case in sciences and the arts, some original ideas and early discoveries remain unexplored; either because they are ahead of their time, or because they have not been presented in a manner or form appropriate for immediate use by employing the tools available then. This was also somewhat true for the aforementioned two approaches: Berdichevskii's approach-deeply rooted in fundamental physics and sophisticated mathematics-has evolved into a generalized variational framework for the mechanics and thermodynamics of microstructures (Berdichevsky, 2008; Berdichevsky, 2009). Aifantis' approach-strongly based on striking similarities and close analogies noted between deformation processes in solids and pattern forming instabilities in other well studied physical systems-was quickly adopted and further developed by the multidisciplinary engineering mechanics and material physics communities, which found applications to many deformation problems across the scale spectrum. It is thus a timely and useful task to re-examine now both approaches, bringing together their advantages and dispensing with their disadvantages. It is a pleasure and an honor to dedicate this article to Victor Berdichevsky: the scientist whom we all still have a lot to learn from and the human being whose endurance, rigor and fairness will remain as a landmark for the generations to come, and for those who are cursed and blessed at the same time to carry out a great tradition away from their homeland.

The paper is delivered in three major sections. In Section 2, the problem of dislocation patterning is discussed by revisiting the original RTD/W–A model with a closer examination on the role of gradient terms in the dynamics, as well as with an elaboration on double slip, and the incorporation of stochastic effects. Section 3 considers generic issues for the problem of dynamic shear banding by incorporating inertia and rate effects in the original stationary model analyzed by the second author and his co-workers for gradient-dependent plastic materials in the softening regime. Section 4 considers instabilities in thin material layers induced by simultaneous action of diffusion and deformation during heteroepitaxial film growth. The paper ends with a number of conclusions listed in Section 5.

2. Dislocation patterning

2.1. The role of gradient terms in dislocation dynamics

(i) *Governing Evolution Equations:* By considering a representative single slip system and distinguishing between immobile or slow mobility forest dislocations with density ρ_s, and mobile or fast moving dislocations with total density $\rho_m = \rho_m^+ + \rho_m^-$ and excess density $k_m = \rho_m^+ - \rho_m^-$, the appropriate mean field evolution equation for the dislocation system at hand may be written in the form

$$\begin{aligned}
\partial_t \rho_s &= -\nabla \mathbf{j}_s + C + \upsilon_s \rho_s \sqrt{\rho_s} - \upsilon_s d_c \rho_s^2 - \beta \rho_s + G(\rho_s)\rho_m, \\
\partial_t \rho_m &= -bB\nabla_x[\bar{\sigma}^{int}(\mathbf{r}) + \sigma^{ext}]k_m + \beta \rho_s - G(\rho_s)\rho_m, \\
\partial_t k_m &= -bB\nabla_x[\bar{\sigma}^{int}(\mathbf{r}) + \sigma^{ext}]\rho_m - G(\rho_s)k_m,
\end{aligned} \tag{1}$$

where $\mathbf{j_s}$ represents the (weak) effective dislocation transport in the forest resulting from thermal mobility and climb, and it will be considered (as in the original W–A model) as diffusive ($\mathbf{j_s} = -D_s \nabla \rho_s$). The quantity C represents a constant source term to be taken equal to zero in the sequel, while the quantity $\upsilon_s \rho_s \sqrt{\rho_s}$ (which could contain a proportionality constant) denotes multiplication of static dislocations within the forest: the density of dislocation sources ρ_s operates with frequency $\upsilon_s \sqrt{\rho_s}$, where υ_s designates the dislocation velocity in the forest. Annihilation of static dislocations is represented by the term $\upsilon_s d_c \rho_s^2$ with d_c denoting a characteristic length for dipole collapse which, in principle, may be evaluated from microscopic analysis (Essmann & Mughrabi, 1979). The coefficient β measures the rate of dislocation freeing from the forest and is associated with the destabilization of dislocation dipoles or clusters under stress. Numerical dislocation dynamics simulations show that in bcc crystals, for example, there is a critical value of externally applied stresses above which dislocation dipoles become unstable (Huang et al., 1999), and this value is a decreasing function of the distance between dipoles. If the forest is considered as an ensemble of dipoles with a mean characteristic width, the threshold stress σ_f for destabilization or freeing, could be extracted from such simulations. More extended numerical analysis could include higher order dislocation clusters and provide the dependence of the threshold stress on the forest dislocation density. The freeing rate should thus be zero below the freeing threshold, and an increasing function of the applied stress above it. Finally, the term $G(\rho_s)\rho_m$ represents the pinning rate of mobile dislocations by the forest. The quantity $G(\rho_s)$ may be represented in the form $G(\rho_s) = \sum_{n \geqslant 1} g_n \rho_s^n$ i.e. the total pinning rate of mobile dislocation by clusters of static ones. The effect of correlation functions, which have been neglected in Eq. (1), will be discussed in Section 2.3.

The quantity b is the magnitude of the Burgers vector, and the quantity B – denoting dislocation mobility – enters in the expression for the gliding velocity υ_g: $\upsilon_g = bB[\sigma^{int}(x) + \sigma^{ext}]$ where $\sigma^{int}(x)$ denotes the local internal stress σ^{ext} and the externally applied one. It then follows (Zaiser et al., 2001) that the average internal stress $\bar{\sigma}^{int}$ in three dimensions is given by the expression

$$\bar{\sigma}^{int}(\mathbf{r}, t) = \int k_m(\mathbf{r}, t)\sigma^{ind}(\mathbf{r} - \mathbf{r_1})d\mathbf{r_1} - \xi \mu b \sqrt{\rho_s} \tag{2}$$

where $\nabla^2 \bar{\sigma}^{int}(\mathbf{r}, t) = [\mu b/(1-\nu)][\partial^3 k_m(\mathbf{r}, t)/\partial_x \partial_y^2]$ with μ being the shear modulus and ν the Poisson's ratio, and the second term in Eq. (2) representing the contribution of pre-existing forest dislocations to the mean internal stress. In this connection, it is noted that the current of mobile dislocation density $\pm\nabla_x(\rho_m^{\pm}\upsilon_g)$ entering in the respective balance laws $\partial_t \rho_m^{\pm} \pm \nabla_x(\rho_m^{\pm}\upsilon_g) = \hat{c}(\rho_s, \rho_m^{\pm})$ reflected in the governing differential system given by Eq. (1), was written in terms of the total stress σ driving these dislocations. [The source term $\hat{c}(\rho_s, \rho_m^{\pm})$ models, in general, dislocation production/annihilation and the gliding velocity υ_g is assumed to depend linearly on σ]. In contrast, the current of immobile dislocations was assumed to be diffusive due to the random motion of these dislocations within the forest (Pontes et al., 2006; Walgraef & Aifantis, 1985a, 1985b).

(ii) *Stability Analysis and Bifurcations:* Two typical approximations may be considered in studying the evolution of dislocation densities during plastic deformation. The first one corresponds to materials with low forest density at the beginning of the deformation process. In this case, the dislocation current which gives rise to the gradient terms in Eq. (1) also contains a contribution resulting from the interaction between gliding dislocations and loops (Gregor & Kratochvil, 1998). As shown there, these terms account for a sweeping mechanism which may be responsible for the early stages of dislocation patterning. The second one, which is considered here, corresponds to materials with a well-developed forest. In this case, advection terms dominate in the gradient terms, as considered in Eq. (1). The consequence of this approximation is to neglect transient patterns which develop during the early stages of the evolution, such as the development of the vein structure, before the formation of PSBs during fatigue. Although we think that these transients should not affect the asymptotic states of the system, it would nevertheless be desirable to incorporate them in the dynamics of Eq. (1), in order to obtain a complete description of pattern evolution. It is now easy to check that Eq. (1) admits the following non-trivial uniform steady state:

$$\sqrt{\rho_s^0} = 1/d_c, \quad \rho_m^0 = (\beta/\gamma)\rho_s^0, \quad k_m^0 = 0, \tag{3}$$

where $\gamma = G(\rho_s^0)$ is the mean effective pinning rate.

The linear stability analysis of this steady state is performed, as usual, by studying the evolution of small nonuniform density perturbations defined as $\hat{\rho}_s = \rho_s - \rho_s^0, \quad \hat{\rho}_m = \rho_m - \rho_m^0, \hat{k}_m = k_m - k_m^0$ The corresponding linear evolution equations in Fourier space are:

$$\begin{aligned}
\partial_t \hat{\rho}_s(\mathbf{q}, t) &= -\left[\tfrac{1}{\tau} - \beta g + q^2 D_s\right]\ \hat{\rho}_s(\mathbf{q}, t) + \gamma \hat{\rho}_m(\mathbf{q}, t), \\
\partial_t \hat{\rho}_m(\mathbf{q}, t) &= -iq_x bB\upsilon_0 \hat{k}_m(\mathbf{q}, t) - \gamma \hat{\rho}_m(\mathbf{q}, t) - \beta g \hat{\rho}_s(\mathbf{q}, t), \\
\partial_t \hat{k}_m(\mathbf{q}, t) &= -\left[\gamma + \tfrac{q_x^2 q_y^2}{q^4} \Lambda\right]\ \hat{k}_m(\mathbf{q}, t) - iq_x bB\upsilon_0 \hat{\rho}_m(\mathbf{q}, t) + iq_x bB\upsilon_0' \hat{\rho}_s(\mathbf{q}, t),
\end{aligned} \tag{4}$$

where $\mathbf{q}$ is the wavevector of the Fourier modes $q^2 = q_x^2 + q_y^2$, $\upsilon_s/2d_c = 1/\tau$, $\upsilon_0 = \left[\sigma^{ext} - \xi\mu b\sqrt{\rho_s^0}\right]$,$\upsilon_0' = (\beta/2\gamma)\xi\mu b\sqrt{\rho_s^0}$,$g = \left(\sum_{n\geqslant 1}(n-1)g_n\rho_s^{0n}\right)/\sum_{n\geqslant 1} g_n\rho_s^{0n}$ and $\Lambda = \left(\mu b^2 B\rho_m^0\right)/[2\pi(1-\nu)]$. Thanks to the finite relaxation rate in Eq. (4)$_3$, $\hat{k}_m(q,t)$ may be adiabatically eliminated, yielding (for the linear term)

$$\hat{k}_m(\mathbf{q},t) = -i\frac{q_x bB\upsilon_0}{\gamma + \left(q_x^2 q_y^2/q^4\right)\Lambda}\ \hat{\rho}_m(\mathbf{q},t) + i\frac{q_x\upsilon_0'}{\gamma + \left(q_x^2 q_y^2/q^4\right)\Lambda}\ \hat{\rho}_s(\mathbf{q},t), \tag{5}$$

and, then, the deduced linear dynamical system becomes:

$$\begin{aligned}\partial_t\hat{\rho}_s(\mathbf{q},t) &= -\left[\tfrac{1}{\tau} - \beta g + q^2 D_s\right]\hat{\rho}_s(\mathbf{q},t) + \gamma\hat{\rho}_m(\mathbf{q},t),\\ \partial_t\hat{\rho}_m(\mathbf{q},t) &= -\left[\gamma + q_x^2 D_m(q)\right]\hat{\rho}_m(\mathbf{q},t) - \left[\beta g - q_x^2 K_m(q)\right]\hat{\rho}_s(\mathbf{q},t).\end{aligned} \tag{6}$$

In a previous analysis (Walgraef, 2002), the glide velocity has been considered as constant. However, we see here that the gradient terms in the mobile dislocation evolution equations do not only generate an effective self-diffusion term with coefficient $D_m = (bB\upsilon_0)^2/\left[\gamma + \Lambda(q_x^2 q_y^2)/q^4\right]$, as in Walgraef (2002), but also an effective forest induced cross-diffusion term with coefficient $K_m = (bB)^2\upsilon_0\upsilon_0'/\left[\gamma + \Lambda(q_x^2 q_y^2)/q^4\right]$.

The eigenvalues of the associated linear evolution matrix are the solutions of the characteristic equation

$$\omega^2 + \omega\left(\frac{1}{\tau} - \beta g + \gamma + D_m q_x^2 + q^2 D_s\right) + \left(\frac{1}{\tau} + q^2 D_s\right)(\gamma + D_m q_x^2) - \beta g D_m q_x^2 - \gamma K_m q_x^2 = 0. \tag{7}$$

When at least one of these eigenvalues has a positive real part, the uniform steady state is unstable. This occurs, in particular, when

$$\beta g + \gamma\frac{K_m}{D_m} > \left(1 + \frac{\gamma}{D_m q_x^2}\right)\left(\frac{1}{\tau} + D_s q^2\right), \tag{8}$$

and the instability threshold corresponds to the minimum of the above defined marginal stability curve.

It follows then, in view also of Eq. (2), that the magnitude of the critical wavevector ($\mathbf{q_c} = q_c\hat{\mathbf{i}}_x$; $\hat{\mathbf{i}}_x$ denotes the unit vector in the slip direction) and the corresponding critical value of the bifurcation parameter β_c is given by the relations

$$q_c = \left(\frac{\gamma}{D_m D_s \tau}\right)^{1/4};\quad \beta_c = \frac{1}{\tau}\left(1 + \sqrt{\frac{\tau\gamma D_s}{D_m}}\right)^2\left\{g + \left[\sigma^i/2(\sigma^{ext} - \sigma^i)\right]\right\}^{-1}, \tag{9}$$

where $\sigma^i = \xi\mu b\sqrt{\rho_s^0}$. This threshold is lower than the one obtained in earlier studies (Walgraef, 2002; Walgraef & Aifantis, 1985a), where the gliding velocity was considered as constant, which rules out cross-diffusion terms in the linear evolution matrix ($K_m = 0$), yielding Eq. (9)$_2$ with the σ^i-dependent term identically equal to zero. If the dominant process for instability corresponds to the pinning of mobile dislocations by static dipoles or junctions ($n = 2$), then Eq. (9) holds with $g \equiv 1$.

(iii) *Nonlinear Analysis:* Close to the pattern forming instability, the dynamics of Eq. (1) may be generically reduced to amplitude equations for the dislocation structure, as discussed in Walgraef and Aifantis (1985a). These equations describe the dynamics of the formation of dislocation walls perpendicular to the primary slip direction and are of the Ginzburg–Landau type. They show that dislocation patterning is very natural in systems where a dynamical equilibrium arises between the freeing of dislocations from the forest and the immobilization of mobile dislocations by the forest or other obstacles. When considering that the gradient terms result in effective diffusion only, the wall structure appears through a supercritical bifurcation which is saturated by scalar cubic nonlinearities. However, even close to instability, the gradient terms of the kinetic equation for the gliding dislocation density may be expanded in series of the perturbations of the uniform steady state, which generates different types of gradient dependent nonlinearities.

On returning now to Eq. (1), we note that after adiabatic elimination of the excess dislocation density k_m, this may be written as

$$\begin{aligned}\partial_t\rho_s &= D_s\Delta\rho_s + C + \upsilon_s\rho_s\sqrt{\rho_s} - \upsilon_s d_c\rho_s^2 - \beta\rho_s + G(\rho_s)\rho_m,\\ \partial_t\rho_m &= \nabla_x[\upsilon_g\tfrac{1}{G(\rho_s)}\nabla_x\upsilon_g\rho_m(\mathbf{r},t)] + \beta\rho_s - G(\rho_s)\rho_m;\quad \upsilon_g = bB[\bar{\sigma}^{int}(\mathbf{r}) + \sigma^{ext}].\end{aligned} \tag{10}$$

which for $n = 2$ (or $g = 1$) gives

$$\begin{aligned}\partial_t\hat{\rho}_s(\mathbf{q},t) &= -\left[\tfrac{1}{\tau} - \beta + q^2 D_s\right]\hat{\rho}_s(\mathbf{q},t) + \gamma\hat{\rho}_m(\mathbf{q},t) + NL_s(\mathbf{q},t),\\ \partial_t\hat{\rho}_m(\mathbf{q},t) &= -\left[\gamma + q_x^2 D_m(q)\right]\hat{\rho}_m(\mathbf{q},t) - \left[\beta - q_x^2 K_m(q)\right]\hat{\rho}_s(\mathbf{q},t) + NL_m(q,t),\end{aligned} \tag{11}$$

where $NL_s(\mathbf{q},t)$ and $NL_m(\mathbf{q},t)$ contain the terms already considered in the original W–A model (Walgraef & Aifantis, 1985b; Walgraef, 2002; Walgraef & Aifantis, 1985a) plus additional contributions generated by the gradient terms which in real space, read

$$NL_m(G) = \left[3\frac{\upsilon_g'}{\upsilon_g} - \frac{G'}{G}\right]\frac{\upsilon_g^2}{G(\rho_s)}(\nabla_x\rho_s)(\nabla_x\rho_m) + \left[\frac{(\upsilon_g')^2}{\upsilon_g^2} - \frac{\upsilon_g' G'}{\upsilon_g G} + \frac{\upsilon_g''}{\upsilon_g}\right]\frac{\upsilon_g^2}{G(\rho_s)}(\nabla_x\rho_s)^2\rho_m. \tag{12}$$

Close to instability, the following order parameter-like equation for unstable modes is obtained

$$\tau_0\partial_t\rho = \left[\varepsilon - d_0\left(q_c^2 + \nabla_x^2\right)^2 + d_\perp\nabla_y^2\right]\rho + \upsilon_0\rho^2 + \upsilon_1(\nabla_x\rho)^2 - u_0\rho^3 - u_1(\nabla_x\rho)^2\rho, \tag{13}$$

where $\tau_0 = \gamma/(q_c^2 D_m\beta_c)$, $\varepsilon = (\beta - \beta_c)/\beta_c$, $d_0 = D_s/q_c^2\beta_c$, $d_\perp = D_s(\gamma + q_c^2 D_m)/(q_c^2 D_m\beta_c)$. The kinetic nonlinear coefficients of this equation may be computed, in principle, from the dynamics of Eq. (10). For the present purposes – which is to describe the qualitative (although generic) behavior of dislocation patterning phenomena – it is sufficient to know that, since $d_\perp > 0$, wavevectors parallel to the x-axis are selected. Then, one may look, as usual, for solutions of the type [(A,A^*) and (B,B^*) are functions of (x,y)]

$$\rho = A\exp(iq_c x) + A^*\exp(-iq_c x) + B\exp(2iq_c x) + B^*\exp(-2iq_c x) + \cdots, \tag{14}$$

which leads to the following evolution equation for the amplitude A (x,y)

$$\tau_0\partial_t A = \left[\varepsilon + 4d_0 q_c^2\nabla_x^2 + d_\perp\nabla_y^2\right]A - u|A|^2 A, \tag{15}$$

where $u = 3u_0 + u_1 q_c^2 + \left[38\upsilon_0(\upsilon_0 + u_1 q_c^2) - 4\upsilon_1^2 q_c^4\right]/(9d_0 q_c^4)$. According to the values of the material parameters and the importance of the gradient contributions, u may thus be positive of negative. For u > 0, which is the case for space-independent diffusion coefficient of mobile dislocations, the bifurcation is supercritical, and the equilibrium pattern amplitude grows as the square root of the deviations of the bifurcation parameter from its critical value. For u < 0, the bifurcation is subcritical, and one should consider higher order nonlinearities to obtain the equilibrium amplitudes. Note that it has been shown that a subcritical Turing bifurcation to stripe patterns is possible in two variable reaction–diffusion models with space-dependent diffusion coefficients (Benson, Maini, & Sherratt, 1997). On the other hand, for increasing ε, the quadratic term of Eq. (13) become relevant, and the pattern amplitude acquires a highly nonlinear profile. This effect needs, however, to be analyzed numerically.

(iv) *Nucleation and Propagation:* It has been experimentally documented (Tabata, Fujita, Hiraoka, & Onishi, 1983) that wall structures, such as persistent slip bands (PSBs), nucleate from material inhomogeneities (veins, grain boundaries, surface defects, local residual strain concentrators, etc.), rather than being induced by thermal fluctuations. In the framework of the amplitude equations formalism of Eq. (15), this corresponds to the front propagation of the patterned state into the unpatterned one from a localized inhomogeneity in the dislocation density. The propagation of such front is governed by its leading edge, and its propagation velocity is well-known (Dee & van Sarloos, 1988). In the present case it is anisotropic, as a result of the anisotropy of the diffusion coefficients of the amplitude equation, with the following properties

$$\upsilon_x = 4q_c\sqrt{d_0\varepsilon}, \quad \upsilon_y = 2\sqrt{d_\perp\varepsilon}, \quad \frac{\upsilon_y}{\upsilon_x} = \frac{1}{2}\sqrt{\frac{d_\perp}{d_0 q_c^2}}. \tag{16}$$

Since $\upsilon_y/\upsilon_x < 1$, the dislocation wall pattern described by Eq. (15) propagates faster in the slip direction than perpendicularly to it. This is schematically shown in Fig. 1. Pattern nucleation through front propagation is also much faster than through fluctuations. This is consistent, for example, with the experimental observation that PSBs nucleate predominantly from residual surface stresses.

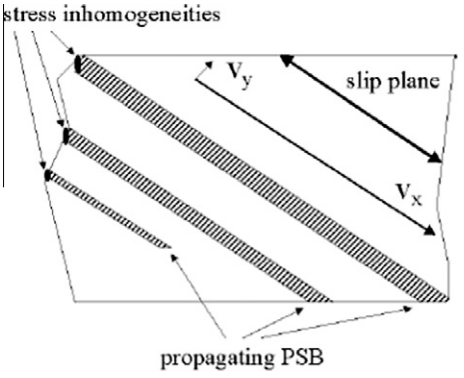

Fig. 1. Schematic representation of the propagation of dislocation wall patterns in a uniform crystal.

2.2. Double slip effects

In this subsection, the original W–A model is extended to consider dislocation mobility along two coexisting slip systems (say, in the directions x and y, orthogonal to each other). In this case the governing differential system consists of coupled rate equations for the stationary or forest (slow moving) and mobile dislocation densities ρ_s and (ρ_{mx}, ρ_{my}). Moreover, as before, each mobile dislocation density population is divided into two subfamilies representing the dislocations gliding in the direction of the Burgers vector (ρ_m^+) and in the opposite one (ρ_m^-), with $\rho_m = \rho_m^+ + \rho_m^-$. The resulting dynamical system may then be written as (with the various coefficients denoting mobility/reaction constants)

$$\begin{aligned}
&\partial_t \rho_s = D_s \Delta \rho_s + \upsilon_s \rho_s \sqrt{\rho_s} - \upsilon_s d_c \rho_s^2 - (\beta_x + \beta_y)\rho_s + \gamma \rho_s^2 (\rho_{mx} + \rho_{my}),\\
&\partial_t \rho_{mx}^+ = -\nabla_x (\upsilon_g \rho_{mx}^+) + \frac{\beta_x}{2}\rho_s - \gamma \rho_s^2 \rho_{mx}^+; \quad \partial_t \rho_{mx}^- = \nabla_x (\upsilon_g \rho_{mx}^-) + \frac{\beta_x}{2}\rho_s - \gamma \rho_s^2 \rho_{mx}^-,\\
&\partial_t \rho_{my}^+ = -\nabla_y (\upsilon_g \rho_{my}^+) + \frac{\beta_y}{2}\rho_s - \gamma \rho_s^2 \rho_{my}^+; \quad \partial_t \rho_{my}^- = \nabla_y (\upsilon_g \rho_{my}^-) + \frac{\beta_y}{2}\rho_s - \gamma \rho_s^2 \rho_{my}^-,
\end{aligned} \tag{17}$$

where, as before, the quantity υ denotes dislocation velocity and the subscripts "s" and "m" designate stationary forest (immobile) and mobile dislocations respectively, while the subscript "g" denotes gliding. It is noted that in the expressions for the dislocation current $\upsilon_g \rho_m$, the gliding velocity was not written in terms of the stresses as in Eq. (1), and that the pinning rate term $G(\rho_s)$ was taken (for simplicity) to be given as in the original W–A model by the formula $G(\rho_s) = \gamma \rho_s^2$.

Under certain conditions for the adiabatic elimination of the fast variable $k_m (\equiv \rho_m^+ - \rho_m^-)$, the following system is obtained for the slow variable $\rho_m \ (\equiv \rho_m^+ + \rho_m^-)$

$$\begin{aligned}
&\partial_t \rho_s = D_s \Delta \rho_s + \upsilon_s \rho_s \sqrt{\rho_s} - \upsilon_s d_c \rho_s^2 - (\beta_x + \beta_y)\rho_s + \gamma \rho_s^2 (\rho_{mx} + \rho_{my}),\\
&\partial_t \rho_{mx} = D_{mx} \nabla_x^2 \rho_{mx} + \beta_x \rho_s - \gamma \rho_s^2 \rho_{mx}; \quad \partial_t \rho_{my} = D_{my} \nabla_y^2 \rho_{my} + \beta_y \rho_s - \gamma \rho_s^2 \rho_{my},
\end{aligned} \tag{18}$$

which is a direct generalization of the original W–A model. It turns out that near bifurcation (as the external stress is increased) the governing equation is of Ginzburg–Landau type of the form

$$\tau_0 \partial_t \rho = \left[\varepsilon - d_0 \left(q_c^2 + \nabla^2\right)^2 - d_\perp \nabla_x^2 \nabla_y^2\right] \rho + \upsilon \rho^2 - u \rho^3, \tag{19}$$

where $\tau_0 = \left(\gamma \rho_s^{0^2}\right)/(q_c^2 D_m \beta_c)$, $\varepsilon = (\beta - \beta_c)/\beta_c$, $d_\perp = \left(\gamma \rho_s^{0^2}\right)/\left[q_c^4 \left(\gamma \rho_s^{0^2} + D_m q_c^2\right)\right]$, $d_0 = D_m/\left(q_c^2 \gamma \rho_s^{0^2}\right)$ and the kinetic coefficients υ and u are explicitly determined from the respective slow-mode dynamics procedure (center manifold theorem). The numerical analysis of Eq. (19) leads to the evolution of the dislocation patterns or "labyrinth structures", as has been explicitly shown in Pontes et al. (2006), in agreement with corresponding experimental observation and transmission electron microscope (TEM) micrographs. The aforementioned simulation results and related experimental observations are depicted in Fig. 2.

2.3. Stochastic effects

The last topic of this section on dislocation patterning concerns the role of stochasticity in deriving more physically-based and mechanism-sensitive evolution equations for the dislocation densities. To this end, we first denote the positions of dislocations in the $(x–y)$ plane (the dislocation lines are assumed to be parallel to the z-axis) by $\mathbf{r}_i(x_i, y_i)$; $i = (1, \ldots, N)$, and the velocity of the ith dislocation υ_i by $\upsilon_i = B\mathbf{b}_i[\tau^{ext}(\mathbf{r}) + \tau^{int}(\mathbf{r})]^{1/m}$, where B is the dislocation mobility, $\mathbf{b}_i$ its Burgers vector, m is the velocity–stress exponent (assumed, for simplicity, equal to unity), $\boldsymbol{\tau}^{int}$ is the internal stress and $\boldsymbol{\tau}^{ext}$ the external resolved shear stress. It is noted here that, for definiteness, we use the shear sress (τ) notation here instead of the (σ) notation. Next, we define the function $f_N(t, \mathbf{r}_1, \ldots, \mathbf{r}_N) d\mathbf{r}_1, \ldots, \mathbf{r}_N$, which gives the probability of finding N dislocations in the volume $d(\mathbf{r}_1, \mathbf{r}_2 \ldots, \mathbf{r}_N)$ in the neighborhood of $(\mathbf{r}_1, \mathbf{r}_2 \ldots, \mathbf{r}_N)$ at time t. By considering dislocations of both positive and negative Burgers vectors $\pm b$ as before, the corresponding dislocation density functions $\rho_\pm = N f_1(\mathbf{r}, t)$ may be introduced by integrating the balance equation for the dislocation number densities over the $(\mathbf{r}_2 \ldots, \mathbf{r}_N)$ subspace to obtain, for the sum $\rho = \rho_+ + \rho_-$ and the difference $k = \rho_+ - \rho_-$, the following dislocation conservation equations

$$\partial_t \rho(\mathbf{r}, t) = -(\mathbf{b}_i \nabla)\{Bk(\mathbf{r}, t)[\tau^{int}(\mathbf{r}) + \tau^{ext}]\}; \quad \partial_t k(\mathbf{r}, t) = -(\mathbf{b}_i \nabla)\{B\rho(\mathbf{r}, t)[\tau^{int}(\mathbf{r}) + \tau^{ext}]\}, \tag{20}$$

where the first equation may be viewed as expressing conservation of the total number of dislocations, while the second equation is a differential statement for the conservation of the net Burgers vector. These local evolution equations may be, in fact, also viewed as the corresponding Langevin equations for stochastic variables. It is also noted that these equations do not contain dislocation reaction terms as the original W–A model does, but such source terms can and should, indeed, be introduced as discussed in Walgraef and Aifantis (2009) and also briefly elaborated upon at the end of this section.

For considering the mean field version of the above equations, the total or overall mean internal stress $\bar{\tau}^{int}$ induced by the dislocation ensemble should be used in Eq. (20). For a system of parallel edge dislocations, the appropriate expression for $\bar{\tau}^{int}(\mathbf{r}) \cong \sum_{j=1}^{N} \tau_j^{ind}(x - x_j, y - y_j)$ may be calculated in terms of the individual stress τ_j^{ind} associated with the j dislocation of Burgers vector b_j; i.e.

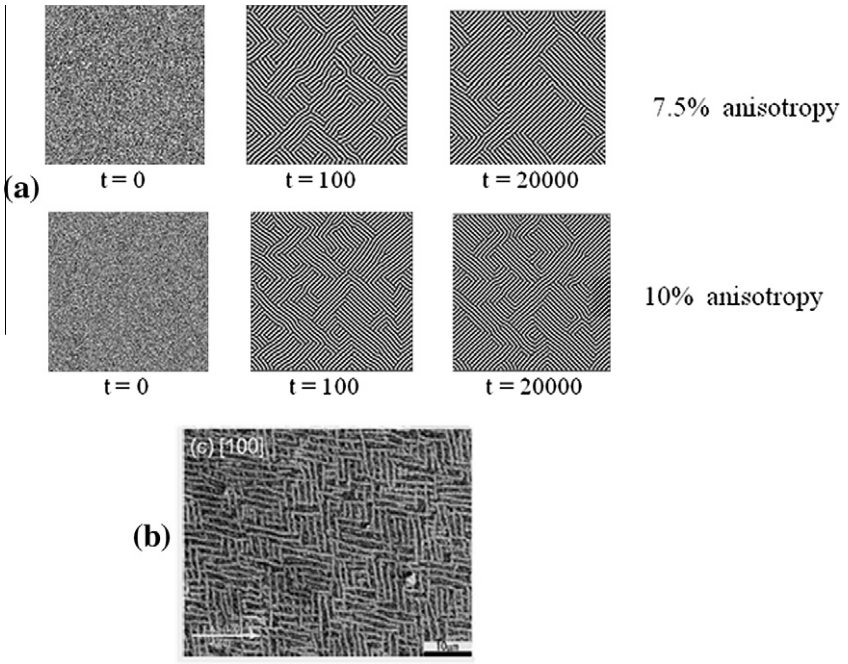

Fig. 2. (a) Temporal evolution of ρ starting from a random initial condition. Primary slip directions are parallel to box diagonals. Walls develop locally perpendicular to each slip direction, domains form and coarsen, finally reaching a steady state which consists of coexisting domains for each wall direction and with most of the domain walls perpendicular to the two slip directions (from J. Pontes, D. Walgraef and E.C. Aifantis, *Int. J. Plast.* **22**, 1486, 2006); (b) Experimental "labyrinth" or "maze" dislocation wall patterns in Cu-single crystal under cyclic loading and oriented for double slip (from Y. Kaneko and S. Hashimoto, *JEOL News* **38**, 20, 2003).

$$\tau_j^{ind}(\mathbf{r}) = -\frac{\mu b_j}{2\pi(1-\nu)}\frac{x(x^2-y^2)}{(x^2+y^2)^2} = -\frac{\mu b_j}{2\pi(1-\nu)}\frac{\partial^3}{\partial_x\partial_y^2}\hat{g}(r); \quad 2\hat{g}(r) = r^2\ln r, \tag{21}$$

where μ is the shear modulus and ν represents the Poisson ratio. The final expression for the mean internal stress $\bar{\tau}^{int}$ is given by

$$\bar{\tau}^{int}(\mathbf{r},t) = \int d\mathbf{r}_1 k(\mathbf{r}_1,t)\tau^{ind}(\mathbf{r}-\mathbf{r}_1); \quad \nabla^2\bar{\tau}^{int}(\mathbf{r},t) = \frac{\mu|\mathbf{b}|}{(1-\nu)}\frac{\partial^3}{\partial_x\partial_y^2}k(\mathbf{r},t). \tag{22}$$

For constant external stress, Eqs. (20) admit the homogeneous stationary solution $[\rho(\mathbf{r},t) = \rho^0, k(\mathbf{r},t) = 0]$. Linear stability analysis for determining the linear evolution of small perturbations $\left[\hat{\rho}(\mathbf{r},t) = \rho(\mathbf{r},t) - \rho^0, \hat{k}(\mathbf{r},t) = k(\mathbf{r},t)\right]$, in the mean field approximation (i.e. neglecting the fluctuating part of the internal stress), leads to the following expressions in the Fourier plane (for B constant and $|\mathbf{b}| = b$)

$$\partial_t\hat{\rho}(\mathbf{q},t) = -iq_x bB\tau^{ext}\hat{k}(\mathbf{q},t); \quad \partial_t\hat{k}(\mathbf{r},t) = -iq_x bB\tau^{ext}\hat{\rho}(\mathbf{q},t) - \frac{q_x^2q_y^2}{q^4}\Lambda\hat{k}(\mathbf{q},t), \tag{23}$$

where $\Lambda = (\mu b^2 B\rho^0)/[2\pi(1-\nu)]$ and the eigenvalues of the corresponding evolution matrix satisfy the equation

$$\omega^2 + \omega\frac{q_x^2q_y^2}{q^4}\Lambda + q_x^2(bB\tau^{ext})^2 = 0. \tag{24}$$

It can easily be seen that the real part of the eigenvalues (i.e. the roots of the above quadratic equation) are always negative and, thus, the uniform solution is stable. As a result, elastic dislocation interaction is not sufficient to induce dislocation patterning; however, uniform dislocation densities are only marginally stable for perturbations with wavevectors parallel or perpendicular to the glide direction. It is noted, in particular, that $\omega = 0$ for spatial modulations perpendicular to the glide direction ($q_x = 0$) which, thus, do not decay (at least linearly). On the other hand, $\omega = \pm\ iq_x bB\tau^{ext}$ for modulations parallel to the glide direction ($q_y = 0$) which, thus, propagate along it. This, which is reminiscent of an analogous argument provided in Walgraef and Aifantis (1985b) (second reference listed there) for both monotonic and cyclic deformations, suggests that the evolution of the dislocation densities is expected to be very sensitive to nonlinear couplings and fluctuations and, thus, a stochastic analysis should be pursued.

To proceed along these lines, the procedure of Walgraef and Aifantis (2009) is adopted by making use of Eq. (21) to derive the corresponding stochastic counterpart of Eq. (20) in the form

$$\begin{aligned}\partial_t\rho(\mathbf{r},t) &= -(\mathbf{b}_i B\nabla)[k(\mathbf{r},t)\tau^{ext} + \int d\mathbf{r_1}\langle k(\mathbf{r},t)k(\mathbf{r_1},t)\rangle\tau^{ind}(\mathbf{r}-\mathbf{r}_1)],\\ \partial_t k(\mathbf{r},t) &= -(\mathbf{b}_i B\nabla)[\rho(\mathbf{r},t)\tau^{ext} + \int d\mathbf{r_1}\langle \rho(\mathbf{r},t)k(\mathbf{r_1},t)\rangle\tau^{ind}(\mathbf{r}-\mathbf{r}_1)],\end{aligned} \tag{25}$$

where $\langle\rangle$ denotes, as usual, the mean value. The mean value of pair densities may be written as $\langle\rho_\alpha(\mathbf{r},t)\rho_\beta(\mathbf{r}_1,t)\rangle = \rho_\alpha(\mathbf{r},t)\rho_\beta(\mathbf{r}_1,t)[1 + d_{\alpha\beta}(\mathbf{r},\mathbf{r}_1)]$; $\alpha,\beta = +$ or $-$, where $d_{\alpha\beta}(\mathbf{r},\mathbf{r}_1)$ is the scaled pair correlation function of dislocation of sign α and β (Zaiser et al., 2001). Then Eq. (25) read

$$\begin{aligned}\partial_t\rho(\mathbf{r},t) &= -(\mathbf{b}_i B\nabla)[k(\mathbf{r},t)\tau^{ext} + \int d\mathbf{r_1}\{k(\mathbf{r},t)k(\mathbf{r_1},t)[1 + d_\Sigma(\mathbf{r},\mathbf{r}_1)] + \rho(\mathbf{r},t)\rho(\mathbf{r}_1,t)d_\Delta(\mathbf{r},\mathbf{r}_1)\}\tau^{ind}(\mathbf{r}-\mathbf{r}_1)], \partial_t k(\mathbf{r},t)\\ &= -(\mathbf{b}_i B\nabla)[\rho(\mathbf{r},t)\tau^{ext} + \int d\mathbf{r_1}\{\rho(\mathbf{r},t)k(\mathbf{r_1},t)[1 + d_\Sigma(\mathbf{r},\mathbf{r}_1)] + k(\mathbf{r},t)\rho(\mathbf{r}_1,t)d_\Delta(\mathbf{r},\mathbf{r}_1)\}\tau^{ind}(\mathbf{r}-\mathbf{r}_1)],\end{aligned} \tag{26}$$

where $2d_\Sigma(\mathbf{r},\mathbf{r}_1) = d_{++}(\mathbf{r},\mathbf{r}_1) + d_{+-}(\mathbf{r},\mathbf{r}_1)$ and $2d_\Delta(\mathbf{r},\mathbf{r}_1) = d_{++}(\mathbf{r},\mathbf{r}_1) - d_{+-}(\mathbf{r},\mathbf{r}_1)$, since $d_{++} = d_{--}$ and $d_{+-} = d_{-+}$. The uniform state $\rho(\mathbf{r},t) = \rho^0$, $k(\mathbf{r},t) = 0$ is still a steady state solution of Eq. (26), and the corresponding linear evolution system of small perturbations reads

$$\begin{aligned}\partial_t\hat{\rho}(\mathbf{r},t) &= -(\mathbf{b}_i B\nabla)[\hat{k}(\mathbf{r},t)\tau^{ext} + \rho^0\int d\mathbf{r_1}\hat{\rho}(\mathbf{r}-\mathbf{r}_1,t)d_\Delta(\mathbf{r}_1)\tau^{ind}(\mathbf{r}_1)],\\ \partial_t\hat{k}(\mathbf{r},t) &= -(\mathbf{b}_i B\nabla)[\hat{\rho}(\mathbf{r},t)\tau^{ext} + \rho^0\int d\mathbf{r_1}\hat{k}(\mathbf{r}-\mathbf{r}_1,t)[1 + d_\Sigma(\mathbf{r}_1)]\tau^{ind}(\mathbf{r}_1)].\end{aligned} \tag{27}$$

The correlation functions d_Σ and d_Δ depend on the scaled variable $\tilde{\mathbf{r}} = \mathbf{r}\sqrt{\rho^0}$ and they exhibit a $1/\tilde{r}$ singularity at small separations, along with an exponential decay at large separations (Zaiser et al., 2001). By further assuming that the dislocation densities are varying smoothly with respect to these correlation functions, the integrals in Eq. (27) may be evaluated through an expansion of the dislocation densities around $\mathbf{r}$. This yields the following expression for the eigenvalues ω of the corresponding linear evolution matrix

$$\omega = \left[\frac{\Lambda}{2}\left(q_x^2 D_+ - q_x^4 E_+ - q_x^2 q_y^2 F_+ - \frac{q_x^2 q_y^2}{q^4}\right)\right] \pm \sqrt{\left[\frac{\Lambda}{2}\left(q_x^2 D_- - q_x^4 E_- - q_x^2 q_y^2 F_- - \frac{q_x^2 q_y^2}{q^4}\right)\right]^2 - q_x^2(|\mathbf{b}|B\tau^{ext})^2}, \tag{28}$$

where $D_\pm = D_\Delta \pm D_\Sigma \approx D_\Delta$, $E_\pm = E_\Delta \pm E_\Sigma \approx E_\Delta$ and $F_\pm = F_\Delta \pm F_\Sigma \approx F_\Delta$, since one may infer from Zaiser et al. (2001) that $d_\Delta >> d_\Sigma$; and the coefficients $(D,E,F)_{\Delta,\Sigma}$ are given in terms of surface integrals involving products $d_{\Delta,\Sigma}$ and third partial derivatives of $\hat{g}(\mathbf{r})$ (Walgraef & Aifantis, 2009). More specifically, the appropriate expression for D_Δ is $D_\Delta = (1/\rho^0)\iint\tilde{x}[d_\Delta(\tilde{\mathbf{r}})\frac{\partial^3 g(\tilde{\mathbf{r}})}{\partial\tilde{x}\partial\tilde{y}^2}]d\tilde{x}d\tilde{y}$, while similar expressions hold for (E_Δ,F_Δ) with the multiplication factors before the integral and the coordinate before the bracket replaced by $(1/6\rho^{0^2},\ 1/2\rho^{0^2})$ and $(\tilde{x}^3,\tilde{x}\tilde{y}^2)$ respectively. It can easily be seen now that both $\hat{\rho}$ and $\hat{k}$ have positive growth rates for finite wavevectors, and that $\hat{\rho}$ has a maximum growth rate which corresponds to $q_y = 0$ and $q_x = \sqrt{D_\Delta/(2E_\Delta)} \propto \sqrt{\rho^0}$. Dislocation walls perpendicular to the glide direction are thus expected to grow first, as obtained in previous numerical simulations. In the presence of an applied external stress, it can easily be established that

- Perturbations with $q_x = 0$ are always marginally stable.
- Perturbations with $q_y = 0$ are unstable for $0 < q_x^2 < q_M^2 = D_+/E_+$, with a growth rate given by

$$\omega = \frac{\Lambda}{2}\left[q_x^2 D_+ - q_x^4 E_+\right] \pm \sqrt{\frac{\Lambda^2}{4}\left[q_x^2 D_- - q_x^4 E_-\right]^2 - q_x^2(|\mathbf{b}|B\tau^{ext})^2} \cong \frac{\Lambda}{2}\left[q_x^2 D_+ - q_x^4 E_+\right] \pm iq_x(|\mathbf{b}|B\tau^{ext}), \tag{29}$$

which is strictly valid for $\tau^{ext} > (\Lambda/bB)q_x\sqrt{D_- - q_x^2 E_-}$. For each wave number between 0 and q_M, there is thus a threshold for the external stress above which the instability is of the wave type and below which it is of the spinodal decomposition type. For sufficiently large external stress, when the bifurcation is of the wave type, walls perpendicular to the glide direction and traveling in this direction are linearly selected; the maximum growth rate occurs (maxRe$[\omega]$) for $q_x^2 = q_0^2 = D_+/(2E_+)$ and the corresponding propagation velocity is $v_0 \cong \pm\, q_c\, bB\tau^{ext}$.

- Perturbations with $q_y \neq 0$ may be unstable.

The above results hold for the case that source terms are not included. The corresponding results for the more realistic case where dislocation reactions are included, as in the W–A model, will be presented in a forthcoming article, along with related details pertaining to the discussion of this section. Here it suffices to mention that in the case that dislocation multiplication/annihilation takes place, the source term $\alpha(\rho) - \beta[\rho^2(\mathbf{r},t) - k^2(\mathbf{r},t)]$ should be added in the r.h.s. of Eq. (26) $_1$, where the stress-dependent nucleation function $\alpha(\rho)$ and annihilation coefficient β have the same physical meaning as the corresponding quantities in Section 2.1, but without considering explicitly the density of forest dislocations ρ_s. Then, an additional constant $a/2$ (resulting from the linearization of the aforementioned source term around the uniform state $\rho^0 \neq 0, k = 0$) enters additively (with a minus sign) in each one of the brackets in the expression for the eigenvalues given

by Eq. (28). The quantity a denotes, indeed, the linear relaxation rate of uniform perturbations and, thus, a^{-1} may be viewed as an effective dislocation lifetime. On the basis of the modified counterpart of Eq. (28), it follows that perturbations with $q_x = 0$ remain only marginally stable, while other ones become stable for short individual dislocation lifetimes. Instability still occurs, in the presence of applied stress, for long dislocation lifetime, such that $a < D_+^2/4E_+$. The maximum linear growth rate still corresponds to $(q_x^2 = q_0^2 = D_+/2E_+, q_y = 0)$. However, the spectrum of unstable wave numbers is now given by $q_x = 0$ and the band $(D_+/2E_+)[1-(1-(4E_+a)/D_+^2)^{1/2}] < q_x^2 < (D_+/2E_+)[1+(1-(4E_+a)/D_+^2)^{1/2}]$. This spectrum does not extend continuously to $q_x = 0$, as in the absence of source terms, although this point still corresponds to a marginal mode. This may induce different nonlinear behavior between the two cases.

We conclude this discussion on dislocation patterning by listing the governing evolution equations resulting by incorporating into the original Walgraef–Aifantis model as expanded upon in Section 2.1, the basic elements of the framework advanced by Zaiser–Groma and co-workers (e.g. (Zaiser et al., 2001)) as elaborated upon in this Section 2.3. The corresponding hybrid W–A/Z–G model reads

$$\begin{aligned}
\partial_t\rho(\mathbf{r},t) &= -(\mathbf{b}_i B\nabla)\{k(\mathbf{r},t)\tau^{ext}\} + \int\{k(\mathbf{r},t)k(\mathbf{r}_1,t)[1+d_\Sigma(\mathbf{r},\mathbf{r}_1)] + \rho(\mathbf{r},t)\rho(\mathbf{r}_1,t)d_\Delta(\mathbf{r},\mathbf{r}_1)\}\tau^{ind}(\mathbf{r}-\mathbf{r}_1)d\mathbf{r}_1 + \alpha + \beta\rho_s(\mathbf{r},t) \\
&\quad - \gamma\rho_s^2(\mathbf{r},t)\rho(\mathbf{r},t), \\
\partial_t k(\mathbf{r},t) &= -(\mathbf{b}_i B\nabla)\{\rho(\mathbf{r},t)\tau^{ext}\} + \int\{\rho(\mathbf{r},t)k(\mathbf{r}_1,t)[1+d_\Sigma(\mathbf{r},\mathbf{r}_1)] + k(\mathbf{r},t)\rho(\mathbf{r}_1,t)d_\Delta(\mathbf{r},\mathbf{r}_1)\}\tau^{ind}(\mathbf{r}-\mathbf{r}_1)d\mathbf{r}_1 \\
&\quad - \gamma\rho_s^2(\mathbf{r},t)k(\mathbf{r},t), \qquad (26^*) \\
\partial_t\rho_s(\mathbf{r},t) &= D_s\Delta\rho_s(\mathbf{r},t) + g[\rho_s(\mathbf{r},t)] - \beta\rho_s(\mathbf{r},t) + \gamma\rho_s^2(\mathbf{r},t)\rho(\mathbf{r},t),
\end{aligned}$$

where (ρ, k) denote as before the (sum, difference) of the gliding dislocation densities, and ρ_s denotes the density of the forest dislocations. A preliminary stability analysis of this system can be found in Walgraef and Aifantis (2009), but a more detailed discussion is postponed for the future as it is beyond the scope of the present article. Nevertheless, some qualitative features of this model are discussed in the last section of the paper.

3. Shear banding

In this section we briefly consider another problem of deformation instability; i.e. the localization of plastic strain in the form of shear bands. As shear bands occur in a variety of materials (metals, polymers, rocks) and scales (macro, micro, nano) this topic is still at the edge of an intense modeling activity. One line of investigation, initiated by Aifantis and collaborators [see, for example, (Aifantis, 1984; Aifantis, 1987) and references therein], is based on the introduction of spatial plastic strain gradients in the relevant softening type or non-convex constitutive equations. Similarly to phase field methods, these gradients allow for smooth strain variations across material interfaces and localization zones, contrary to classical theories giving discontinuous profiles. In particular, strain gradients can conveniently model the heterogeneity of plastic flow, allow for non-vanishing critical wavelengths characterizing the onset of instability of uniform deformations and enable explicit computations of shear band profiles (Zbib & Aifantis, 1988). Up to now, however little attention has been given to the dynamics of localization and the evolution of shear band profiles, especially when multiple shear bands occur. Multiple shear banding is routinely observed in amorphous and nanocrystalline materials as shown, for example, in Fig. 3. Hence, the aim of this part of the paper is to discuss this problem and to propose a framework to address it. A few conjectures are proposed, as well as guidelines to analyze them. The analysis provided below is rather qualitative and restricted to one dimension only. A more elaborate treatment should incorporate at least two families of shear bands evolving in two different directions, in analogy to the double slip case discussed in the previous section for dislocation populations.

3.1. Governing equations in one-dimension

Let us consider the governing one-dimensional differential equations for the simple shearing of a viscoplastic material within the strain gradient theory, i.e.

$$\partial_t\epsilon = \partial_x\upsilon; \quad \rho\partial_t\upsilon = \partial_x\tau; \quad \tau = \kappa(\epsilon,\dot{\epsilon}) - c\partial_x^2\epsilon, \qquad (30)$$

where τ, ϵ denote stress and strain ($\epsilon = \partial_x u$; u is the displacement), while ρ, υ denote material density and velocity ($\upsilon = \partial_t u$), and x is the spatial coordinate orthogonal to the shear stress ($0 < x < L$). The last statement in Eq. (30) is a strain gradient-dependent constitutive equation where is a nonlinear function of and, which may exhibit material softening in both quantities; i.e. the graph $\kappa = \kappa(\epsilon,\dot{\epsilon})$ may contain branches where $\partial\kappa/\partial\epsilon$ or $\partial\kappa/\partial\dot{\epsilon}$ may be negative. Higher-order spatial effects are taken into account through the gradient dependence upon the coefficient c, which may be written as $c = \mu l^2$, where μ is the shear modulus and l is an internal material length. Neither thermal effects nor orientational aspects are considered here for simplicity. For a material where the softening curve of the homogeneous part of the flow stress has the form of Zbib and Aifantis (1988),

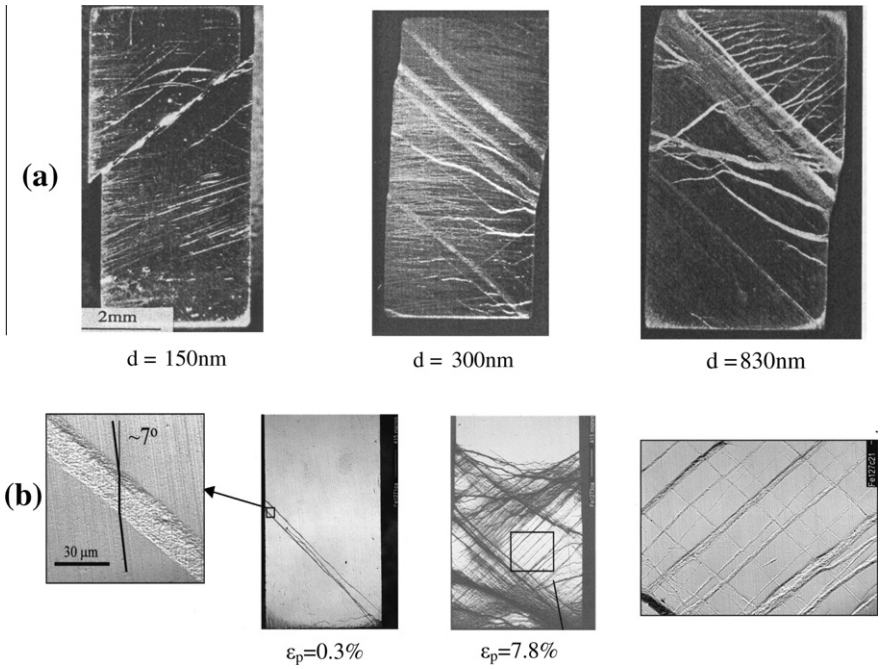

Fig. 3. Shear band patterns for ultrafine grain (ufg) and nanocrystalline (nc) bulk polycrystals under compression. **(a)** Fe-10%Cu bulk polycrystals with average grain size d = (150, 300, 830 nm) (from Carsley, J. E., Fisher, A., Milligan W. W., & Aifantis, E. C., (1998). Mechanical behavior of a bulk nanostructured iron alloy. *Metallurgical and Materials Transactions A, 29A*, 2261–2271); **(b)** Fe bulk polycrystals with an average grain size of ~270 nm at plastic strain levels 0.3% and 7.8% respectively (from D. Jia, K.T. Ramesh and E. Ma, Effects of nanocrystalline and ultrafine grain sizes on constitutive behavior and shear bands in iron, *Acta Materialia* **51**, 3495–3509, 2003).

$$\tau_{\text{hom}} = \tau_m - \alpha(\epsilon - \epsilon_m)^2, \tag{31}$$

with α denoting a constant and (τ_m, ϵ_m) denoting the maximum point of the homogeneous part of the stress–strain curve, Eq. (30) yields the following fourth-order partial differential equation

$$\rho\partial_x^2\epsilon = \partial_x^2[\kappa(\epsilon,\dot{\epsilon}) - c\partial_x^2\epsilon] = s\partial_x^2\partial_t\epsilon - \alpha\partial_x^2(\epsilon-\epsilon_m)^2 - c\partial_x^4\epsilon, \tag{32}$$

where the strain rate sensitivity parameter $s = \partial\kappa/\partial\dot{\epsilon}$ is assumed here to be constant. The softening curve may have more elaborate and physically-realistic forms, e.g. as in Zbib and Aifantis (1988).In any case it is noted that Eq. (32) has the structure of a generalized Cahn–Hilliard equation. One may thus expect that its solution could reproduce some aspects of spinodal decomposition.

3.2. Linear stability & nonlinear analysis

(**i**) *Linear Stability and First Stages of Localization.* First we note that Eq. (32) is conservative and admits any physically realizable uniform strain distribution, ϵ_0, as a steady state solution. According to its stability, this solution may or may not evolve towards a non uniform one, $\epsilon_s(x)$, but the quantity $\frac{1}{L}\int \epsilon_s(x)dx = \epsilon_0$ is conserved. In the hardening domain ($\epsilon < \epsilon_m$), uniform strains are stable, while in the softening domain ($\epsilon > \epsilon_m$), uniform strains are unstable versus spatial modulations with wavevectors q, such that $0 \leqslant q^2 \leqslant q_M^2 = 2\alpha(\epsilon_0 - \epsilon_m)/c$. Unstable modes with wavevectors q_0, such that $q_0^2 = \alpha(\epsilon_0 - \epsilon_m)/c$, have the maximum growth rate.

To proceed further, we next note that the range of unstable wavevectors depends crucially on the strain gradient coefficient c. Although one may always consider it as an adjustable parameter, it would be important for the predictability of the theory to evaluate this parameter independently. As in spinodal decomposition, the system evolution starts by developing spatial modulations corresponding to the maximum growth rate of the linear theory. However, nonlinear effects and mode couplings become rapidly important, and deviations from this behavior increase. One of the main interesting questions is then to determine the evolution of the strain profile $\epsilon(x,t)$.

(**ii**) *Nonlinear Analysis and Shear Band Evolution*: In the case of Cahn–Hilliard dynamics, the initial periodic perturbations of the unstable state become soon destabilized with respect to modes with larger wavelengths (San Miguel, Montagne, Amengual, & Hernandez, 1996). The system then evolves through successive transitions to a state which cannot be described any more as a spatially periodic state with a well defined wavelength, but as a set of coexisting localized domains, or "bubbles". In the present case, these bubbles, which are soft domains, connect unstable high strain states and the stable low strain

states. Their stability is thus a crucial issue. The final dynamics of the system is then governed by the evolution of these domains, induced by their mutual interactions.

An elegant approach to this problem has been presented recently for the one-dimensional Cahn–Hilliard equation in Calisto, Clerc, Rojas, and Tirapegui (2000). They show that, due to the conservative nature of the order parameter, the interaction between bubbles does not induce annihilation by recombination, as in systems with non conserved order parameters. Instead, small bubbles shrink and disappear while larger bubbles grow in order to conserve the total surface allowed to corresponding phase. The asymptotic situation corresponds then to a limited domain of one phase, embedded in the other phase, which occupies the remaining space. In the present case, this could be the "shear band" solution of Zbib and Aifantis (1988), i.e.

$$\epsilon(x) = \epsilon_m + \delta[3\ sech^2(\xi x) - 1], \tag{33}$$

where $\delta = \sqrt{\frac{\tau_m - \tau_0}{\alpha}}$ and $\xi = \sqrt{\frac{\alpha}{2c}}\delta$, with $\tau_m - \alpha(\epsilon - \epsilon_m)^2 = \tau_0$. This solution corresponds to the fact that, if one imposes a strain ($\epsilon_0 > \epsilon_m$) on a system described by the softening curve of Eq. (31), it decomposes in a high strain domain of width of the order of ξ^{-1}(where the maximum strain is $\epsilon_2 = \epsilon_0 - \delta$) and the remaining space (where the strain is $\epsilon_1 = \epsilon_0 - 2\delta$).

3.3. Nonuniform materials and multiple shear bands

When uniform strain reaches instability, unstable modes start growing, which induces the nucleation of shear bands. Although the growth of unstable modes may always be randomly induced by fluctuations, it usually starts preferentially at local defects or weak zones. In this case, the spatial pattern propagates into the system through a front propagation process. In the same spirit, the presence of local hard zones may hinder or stop spatial modes propagation. On the other hand, the presence of hard zones between neighboring bands should limit coarsening by impeding their coalescence. As a result, in such two-phase materials, regular distributions of hard zones should favor multiple shear banding. This situation may be described by the model of Eq. (32) where ϵ_m varies periodically between a minimum (ϵ_W) and a maximum (ϵ_h) value, which correspond to weak and hard zones respectively. Then Eq. (32) becomes

$$\rho\partial_t^2\epsilon = \partial_x^2[\kappa(\epsilon,\dot{\epsilon}) - c\partial_x^2\epsilon] = \partial_x^2\left[s\partial_t\epsilon + \tau_m - \alpha(\epsilon - \epsilon_w - \Delta(x))^2 - c\partial_x^2\epsilon\right], \tag{34}$$

where ϵ_w is constant and $\Delta(x)$ is a positive periodic function with wave number q_1. This yields, for linear evolution of perturbations $\hat{\epsilon}(x)$ from a uniform strain ϵ_0,

$$\rho\partial_t^2\hat{\epsilon} = \partial_x^2\left[s\partial_t - 2\alpha(\epsilon_0 - \epsilon_m(x)) - c\partial_x^2\right]\hat{\epsilon} = \partial_x^2\left[s\partial_t - 2\alpha(\epsilon_0 - \epsilon_w - \Delta(x)) - c\partial_x^2\right]\hat{\epsilon} \tag{35}$$

For ($\epsilon_0 < \epsilon_w$), the uniform strain remain stable, but for $\epsilon_w < \epsilon_0 < \epsilon_h$, it is only locally unstable and one may consider $\Delta(x)$ as an external modulation imposed on the system. Close to instability, the dynamics may be reduced to an amplitude equation for the fastest growing mode, with wave number q_0, in the presence of an external forcing of wave number q_1. It is now well known that for $q_1 > 4q_0$, the resonance between external forcing and fastest growing mode is weak. If, furthermore, $q_1 > 4\sqrt{2}q_0$ (or $\lambda_0 > 4\sqrt{2}\lambda_1$), the coupling with any unstable mode is weak and will not affect significantly the resulting spatial pattern. One may thus expect that in this case, the scenario described earlier (which finally leads to one final shear band in the system) remains valid.

On the contrary, if $q_1 < 4q_0$ (or $\lambda_0 < 4\lambda_1$), strong resonances may occur between external forcing and unstable modes. For resonant forcing ($q_1 = nq_0(n¡4)$), the pattern wavelength should remain locked to a multiple of the forcing wavelength ($\lambda_0 = n\lambda_1(\lambda_0 = n\lambda_1)$). For non resonant forcing, commensurate–incommensurate structures develop, which consist in layered domains, where the wavelength is locked, separated by domain walls, where the phase of the pattern changes abruptly (Walgraef, 1996). In this case, coarsening can hardly occur and arrays of shear bands are expected to remain in the system, which confirms the link between material heterogeneity and multiple shear bands.

These considerations should be put in parallel with numerical simulations of shear band formation in a heterogeneous material with weak zones (Shi, 2004). In this work, it is observed that, for densely distributed weak zones (i.e., the spacing between weak zones is less than shear bandwidth), nearby shear bands coalesce to form a single larger shear band. Once a dominant shear band is formed, the other shear bands start to unload. For sparsely distributed weak zones (i.e., the spacing between weak zones is larger than the shear bandwidth), separated shear bands occur simultaneously, which confirms that the distribution of weak zones plays an important role in the shear band formation.

4. Deformation instabilities in heteroepitaxial film growth

The combination of atomic deposition and nonlinear diffusion may lead, below a critical temperature, to the instability of uniform deposited atomic layers. This instability may trigger the formation of self-assembled nanostructures which correspond to regular spatial variations of the substrate coverage. Since film-substrate lattice misfits coverage inhomogeneities generate internal stresses, the coupling between deposition dynamics and film elasticity fields has to be considered. For stable uniform layers in the high and low temperature limits, this coupling may be neglected. Nevertheless, elastic deformation instabilities may be induced by compressive misfit strains only. These could lead to square deformation patterns, on the

surface of isotropic films thinner than the critical thickness for misfit dislocation generation. For intermediate temperatures, this coupling is destabilizing and may generate triangular or hexagonal deformation patterns as well. At low coverage these patterns correspond to arrays of dots, as in Stranski–Krastanov growth, although their formation here is dynamically driven.

4.1. The dynamics of a deposited layer on a substrate

The derivation of the deformation dynamics of a thin film on a substrate, in the presence of a spatially varying defect concentration field has already been presented in Walgraef, Ghoniem, and Lauzeral (1997). The evolution equation for the film bending coordinate can be adapted to the present case where various structural defects (vacant sites, deposited atoms and adatoms, islands, grains, etc.) induce lattice dilatation (positive or negative) in the deposited layer. It may be written in the form of a von Karman model which can be shown to yield

$$\partial^2\xi + \eta\partial_t\xi + \frac{Eh^2}{12\rho(1-\nu^2)}\Delta^2\xi - \frac{1}{2\rho}\sigma_{\alpha\beta}\xi_{,\alpha\beta} = \frac{\theta}{b^3\rho h}(c_+ - c_-) - \frac{\kappa}{\rho h}\xi. \tag{36}$$

Here ξ is the bending coordinate of the film of thickness h; η is a structural viscosity coefficient which takes care of the dissipation effects due to film-substrate interactions; c_+ and c_- are the atomic concentrations at the layer top and bottom surfaces, respectively; and κ is the adhesive bond stiffness constant defined by $F(\xi) = -\kappa\xi$, where $F(\xi)$ denotes the adhesive force (per unit surface) between film and substrate: this force may be represented by the universal bonding curve, usually invoked in process zone fracture models (Needleman, 1990), and is approximated here by a linear dependence in ξ (which is justified for small displacements); z is the film coordinate perpendicular to the substrate surface with (x,y) denoting the planar coordinates parallel to the substrate surface; σ_{ij} is the stress tensor (ϵ_{ij} is the strain tensor); $\xi_{,ij}$ stands for $\partial^2\xi/\partial x\partial y$ with $\Delta = \nabla_x^2 + \nabla_y^2$; while E is the film's Young modulus and ν its Poisson ratio. Finally, if E^0 stands for the self-energy of deposited atoms, then $E^0 \approx \theta$ with $\theta \approx 0.3b^3K$, where b is the Burgers vector magnitude and K the bulk elasticity modulus. The components of the in-plane stress tensor σ_{ij} are given by Walgraef et al. (1997)

$$\sigma_{ii} = \frac{E}{2(1-\nu)}\epsilon_m + \frac{E}{2(1-\nu^2)}(\xi_{,i}^2 + \nu\xi_j^2); \quad \sigma_{ij} = \frac{E}{1+\nu}\xi_{,i}\xi_j, \tag{37}$$

where, as before $i = x$ (or y) and $j = y$ (or x), while ϵ_m denotes the misfit strain induced by the substrate on the deposited layer in isotropic conditions. The schematic representation of the physical configuration considered is shown in Fig. 4.

The governing differential relation given by Eq. (36) shows that the film's bending evolution is coupled to the atomic coverage at the top and bottom film surfaces. In a previous publication (Walgraef, 2003), the growth of a deposited film on a substrate has been described by a reaction–diffusion model, based on atomic adsorption, desorption and diffusion. In this description, the space–dependent coverage at the bottom film surface tends to $c_- \approx 1$, while $c_+ = c_0\varphi_+(\mathbf{r},t)$. The evolution of φ_+ may also be obtained from this model, and the relevant dynamical system becomes

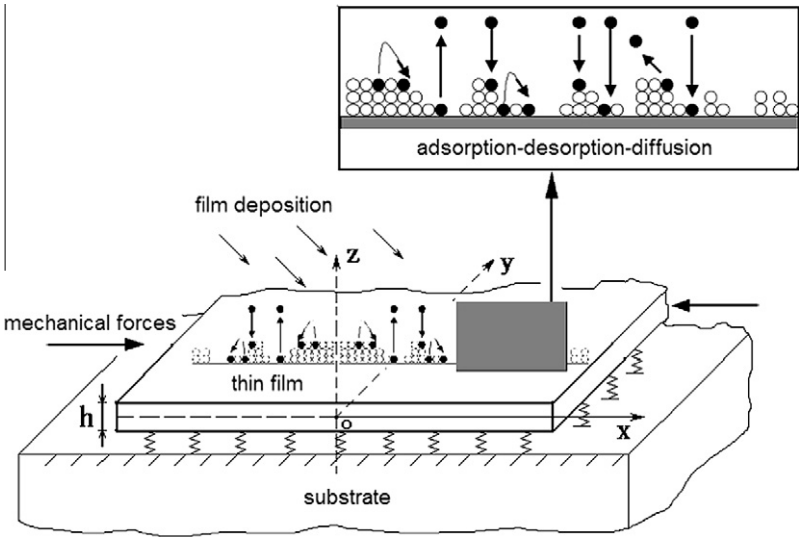

Fig. 4. Schematic representation of the basic mechanisms and geometric factors involved during deposition of an elastic film in a rigid substrate.

$$\partial_t^2\xi+\eta\partial_t\xi=-\frac{Eh^2}{12\rho(1-\nu^2)}\Delta^2\xi+\frac{1}{2\rho}\sigma_{\alpha\beta}\xi_{,\alpha\beta}-\frac{\kappa}{\rho h}\xi+\frac{\partial c_0}{b^3\rho h}(\phi_+-1),\tag{38}$$

$$\partial_t\phi_+=\frac{1}{\tau}(1-\phi_+)\phi_++D_h\nabla^2\left[\frac{1}{c_0}\ln\frac{\phi_+}{1-c_0\phi_+}-\frac{\epsilon_0}{k_BT}\phi_+-\frac{\xi_0^2}{k_BT}\nabla^2\phi_++\frac{mh\theta}{2c_0k_BT}\nabla^2\xi\right],$$

where $c_0=\frac{\alpha-\beta}{\alpha}$ and $\tau^{-1}=\alpha-\beta$, with α and β denoting the adsorption and desorption rates, respectively; D_h is the lateral diffusion coefficient; $\epsilon_0=n\epsilon$ and $\xi_0^2=na^2\epsilon$, where ϵ is the atomic pair interaction energy, n is the lattice coordination number and a is the lattice constant. Fickean diffusion and local thermodynamic equilibrium have been considered in the derivation of Eq. (38); and for the sake of simplicity, surface diffusion and misfit strains have been considered as isotropic.

4.2. Deformation instabilities in a monoatomic layer

The system of Eq. (38) admits a uniform steady state, $\phi_+=1,\xi=0$, which corresponds to a uniform and undeformed deposited layer. Its stability versus inhomogeneous coverage and deformation perturbations is given by the linear evolution of small perturbations $\phi=\phi_+-1$ and ξ, which in Fourier space may be written as

$$\begin{aligned}\tau\partial_t\varphi_q&=-[1+\Gamma(1-\mu)q^2+q^4a^2\Gamma\mu]\varphi_q+q^4\frac{mh\theta D_h\tau}{2c_0k_BT}\xi_q,\\ \partial_t^2\xi_q+\eta\partial_t\xi_q&=-\left[\frac{Eh^2}{12\rho(1-\nu^2)}q^4+\frac{E}{4\rho(1-\nu)}\epsilon_mq^2+\frac{\kappa}{\rho h}\right]\xi_q+\frac{\theta c_0}{b^3\rho h}\varphi_q,\end{aligned}\tag{39}$$

where $\Gamma=\frac{D_h\tau}{c_0(1-c_0)}$ and $\mu=\frac{c_0(1-c_0)\epsilon_0}{k_BT}$.

At sufficiently high and low temperatures, uniform atomic coverage which evolves through adsorption–desorption processes and nonlinear diffusion on the substrate, is known to be stable. This is due to the fact that the factor $\frac{D_h\tau}{k_BT}$ in the coverage evolution equation, i.e. Eq. (38), tends to zero in the high and low temperature limits (Walgraef, 2003). Similarly, the coupling between film bending and coverage fluctuations becomes irrelevant in these limits, where the system may thus be described by the evolution of the bending coordinate only. In isotropic systems, its linear evolution is given by the equation

$$\partial_t^2\xi_q+\eta\partial_t\xi_q=-\left[\frac{Eh^2}{12\rho(1-\nu^2)}q^4+\frac{E}{4\rho(1-\nu)}\epsilon_mq^2+\frac{\kappa}{\rho h}\right]\xi_q.\tag{40}$$

In this case, undeformed layers are unstable for compressive misfit strains $\left(\epsilon_m\propto\frac{a_s-a_f}{a_f}<0\right)$, such that

$$\epsilon_m<-\left[\frac{h^2}{3(1+\nu)}q^2+\frac{4(1-\nu)\kappa}{q^2Eh}\right]<-2\frac{h^2(1-\nu)}{3(1+\nu)}q_c^2=-4\sqrt{\frac{h\kappa}{3E(1-\nu)}\frac{(1-\nu)}{(1+\nu)}}=-\epsilon_c,\tag{41}$$

where $q_c=\left(\frac{12\kappa(1-\nu^2)}{Eh^3}\right)^{1/4}$. On the other hand, for larger misfits ($|\epsilon_m|>|\epsilon_c|$), the linear growth rate is maximum for spatial modulations of wavenumber q_0 and the corresponding preferred wavelength λ_0 is given by the relations

$$q_0=\frac{1}{h}\sqrt{\frac{3(1+\nu)|\epsilon_m|}{2}};\quad \lambda_0=2h\pi\sqrt{\frac{2}{3(1+\nu)|\epsilon_m|}}.\tag{42}$$

Deformation patterns are thus expected to develop beyond instability (i.e. for $|\epsilon_m|>|\epsilon_c|$), according to the nonlinear elasticity equation, which in real space, reads

$$\begin{aligned}\partial_t^2\xi_q+\eta\partial_t\xi=&-\left[\frac{Eh^2}{12\rho(1-\nu^2)}\Delta^2+\frac{E}{4\rho(1-\nu)}\epsilon_m\Delta+\frac{\kappa}{\rho h}\right]\xi\\&+\frac{E}{4\rho(1-\nu^2)}\left[\left(\xi_{,x}^2+\nu\xi_{,y}^2\right)\xi_{,xx}+4(1-\nu)\xi_{,x}\xi_{,y}\xi_{,xy}+(\xi_{,y}^2+\nu\xi_{,x}^2)\xi_{,yy}\right],\end{aligned}\tag{43}$$

or

$$\partial_T^2\zeta+\tau_0\partial_T\xi=\left[\epsilon-\frac{1}{q_c^4}\left(q_0^2+\Delta\right)^2\right]\zeta+\frac{3}{q_c^4}[(\zeta_{,x}^2+\nu\zeta_{,y}^2)\zeta_{,xx}+4(1-\nu)\zeta_{,x}\zeta_{,y}\zeta_{,xy}+(\zeta_{,y}^2+\nu\zeta_{,x}^2)\zeta_{,yy}],\tag{44}$$

where $T=\sqrt{\frac{\kappa}{h\rho}}t,\tau_0=\eta\sqrt{\frac{h\rho}{\kappa}},\epsilon=\frac{\epsilon_m^2-\epsilon_c^2}{\epsilon_c^2}$ and $\zeta=\frac{\xi}{h}$. The simplest patterns may be thought of as one-dimensional deformations of preferred wavevector arbitrarily oriented (without loss of generality) parallel to the x-axis, and such that $\zeta=A(x,y)\exp(iq_0x)+c.c.$, with c.c. denoting comlex conjucate. Their amplitude equation reads:

$$\tau_0\partial_TA=\epsilon A+4\frac{q_0^2}{q_c^4}\partial_x^2A-\frac{1}{q_c^4}\partial_y^4A-gA|A|^2,\tag{45}$$

which is valid close to instability and describes the evolution of the system on asymptotic space and time scales ($x \approx 1/\sqrt{\epsilon}, y \approx 1/\epsilon^{1/4}, t \approx 1/\epsilon$) (Walgraef, 1996). Hence, close to instability, the second time derivative of the von Karman equation is scaled by ϵ^2 and may be neglected with respect to the dominant of order ϵ terms. In this regime, this term can only contribute if dissipative effects are vanishingly small, and can be scaled as $\sqrt{\epsilon}$ (the time scale being set by $t \approx 1/\sqrt{\epsilon}$). This equation gives, as uniform steady state solution, $|A_0| = \epsilon/g$. The stability of this solution versus spatial modulations of critical wavevector making an angle ψ with the x-axis may be studied through amplitude equations of the form

$$\zeta = A exp(iq_0 x) + B exp[iq_0(x\cos\psi + y\sin\psi)] + c.c.,$$

which may be written (for uniform amplitudes) as

$$\tau_0 \partial_T A = \epsilon A - gA(|A|^2 + \gamma(\psi)|B|^2); \quad \tau_0 \partial_T B = \epsilon B - gB(|B|^2 + \gamma(\psi)|A|^2), \tag{46}$$

where $g = 3\frac{q_0^4}{q_c^4}$ and $\gamma(\psi) = [2\ v + 2(1-v)\cos^2(\psi)]$.

One-dimensional deformation patterns $|A_0| = \epsilon/g$ are thus unstable, since $\gamma(\psi) < 1$ for a range of angles ψ such that $\cos^2(\psi) < \frac{1-2v}{2(1-v)}$. Furthermore, since $\gamma(\psi)$ is minimum for $\psi = \frac{\pi}{2}$, selected patterns should correspond to square planforms such that $\zeta = A(x,y)exp(iq_0x) + B(x,y)exp(iq_0y) + c.c.$ with amplitude equations

$$\begin{aligned} \tau_0 \partial_T A &= \epsilon A + 4\frac{q_0^2}{q_c^2}\partial_x^2 A - \frac{1}{q_c^4}\partial_y^4 A - gA(|A|^2 + 2v|B|^2), \\ \tau_0 \partial_T B &= \epsilon B + 4\frac{q_0^2}{q_c^2}\partial_y^2 B - \frac{1}{q_c^4}\partial_x^4 A - gB(|B|^2 + 2v|A|^2), \end{aligned} \tag{47}$$

and steady states $|A_s|^2 = |B_s|^2 = \frac{\epsilon}{g}\frac{1}{(1+2v)} = \frac{\epsilon_m^2 - \epsilon_c^2}{3(1+2v)\epsilon_m^2}$.

5. Conclusions and outlook

We showed in this paper that the rate equation or reaction-transport-diffusion (RTD) approach provides a qualitative description of the behavior of forest and mobile dislocation densities in crystalline materials under loading. It is shown how plastic deformation and dislocation patterning occur as the result of a dynamical equilibrium between dislocation freeing and immobilization in the forest (similar behavior should be obtained on replacing the forest by sub-boundaries or other obstacles to dislocation motion).The analysis illustrates the effect of the glide system (single and double slip) on the pattern structure. It justifies the fact that the combination of dislocation glide and interactions with the forest leads to an effective diffusive motion of mobile dislocations. It relates wavelength selection, deformation band growth and propagation to relevant materials parameters. It allows to test the effect of different physical mechanisms or loading processes on instability thresholds, pattern nucleation, selection and stability. It is necessary, however, to access the relation of this approach to the dominant microscopic underlying mechanisms or, in other words, to determine its position in the framework of multiscale modeling. Although the proposed method describes the collective behavior of dislocation populations, it is based on elementary dynamical events between few dislocations. Hence, the corresponding kinetic coefficients, cross-sections, annihilation and characteristic interaction lengths may be provided by microscopic numerical computations. The determination of reliable kinetic coefficients in the rate equations may not only improve quantitatively the results, but also their incorporation in macroscopic descriptions. A rather new feature was the introduction of stochastic elements of the Groma–Zaiser type into the original Walgraef–Aifantis model. The resulting improved hybrid model is able to reproduce dislocation clustering for low external stress and low forest density. However, on increasing stress, inhomogeneous dislocation distributions transform into wall patterns with the walls being perpendicular to the glide direction. This qualitative change is due to the fact that, at low stress, the dynamics is conservative and of the spinodal decomposition type, while at high stress, forest dislocations become important and a dynamical equilibrium between dislocation freeing and immobilization sets in. This triggers an instability of the Turing type where the combination of dislocation glide and pinning within the forest leads to an effective diffusive motion of mobile dislocations, as in the case when stochastic effects were neglected. However, this effective diffusion coefficient becomes space dependent through its dependence on the forest density. Hence spatial non uniformity of this density may strongly affect the nucleation and stability of wall patterns.

Another topic discussed in the paper was concerned with dynamic shear banding. An explicit stress-stain curve with a softening region was considered and strain gradient terms are included in the model. For unstable uniform strains, the second strain gradient acts as a stabilizer versus short wavelength modulations. Based on the fact that the mean strain is conserved and on similarities with spinodal decomposition, a scenario is proposed for the evolution of spatial modes. For short times, a regular array of bands develop, with a separation distance selected by linear effects. When time goes on, coarsening occurs and thin bands disappear at the expense of thicker ones. Finally, one band remains the width and profile of which is determined by the corresponding material parameters and the initial uniform strain. In heterogeneous materials, weak zones act preferentially as nucleation centers for deformation bands. Hard zones, on the contrary, may suppress deformation propagation and band coarsening. For regularly distributed weak zones, it is anticipated that multiple shear banding is favored when the spacing between weak zones becomes comparable or larger than the separation between bands. This preliminary discussion is also based on generic arguments of pattern formation theory. It should be checked explicitly, both analytically and numerically, for appropriate material parameters, stress–strain curves and flow stress expressions.

The last topic considered in the paper was concerned with the evolution of a growing monoatomic layer, deposited on a substrate.This evolution has been described by a dynamical model of the reaction–diffusion type, coupled with internal stresses, generated by coverage or concentration variations and misfit strains induced by the film-substrate coupling. In this description, the coupling between surface coverage variations and deformation field is destabilizing. Below the critical thickness for nucleation of misfit dislocations, this coupling may induce regular deformation patterns. Well above the critical temperature of adsorbed layer instability, pattern formation may be induced by compressive misfit stresses only. Preferred structures should correspond in this case to square lattices in isotropic systems. For lower temperatures, but still above the adsorbed layer instability temperature, the coupling between coverage inhomogeneities and film deformation is twofold: on one hand, it enlarges the linear instability domain; on the other hand, it adds new contributions to the nonlinear terms of the dynamics and, in particular, quadratic ones. As it will be discussed in detail in a follow-up article, these contributions may modify the selected deformation patterns. Effectively, when coverage nonlinearities dominate, stable patterns should correspond to hexagons, or wrinkles. When elastic nonlinearities dominate, stable patterns should correspond to squares or hexagons. In this case, the amplitude of the deformation pattern is larger for squares than for hexagons. For ultrathin films, the results derived within this approach are reminiscent of Stranski–Krastanov growth, although they are strongly dependent on dynamical aspects. Furthermore, instability thresholds, critical temperatures, wavelengths, buckle amplitudes etc., may be explicitly expressed as functions of kinetic rates and material parameters. Hence, quantitative results may be obtained for specific systems, which could allow comparisons with experimental data.

Despite of the drawbacks related to the mathematical difficulties in the nonlinear regime and the rather little attention to the physical mechanics at the atomic and subatomic scale, the present approach may be viewed as a compromise between molecular/discrete dislocation dynamics (MD/DDD) simulations and more complex dislocation-density tensor based theories which are not yet well-suited for interpreting dislocation and, more generally, deformation patterning phenomena. The analytical results obtained from linear stability analysis provide a useful guide for understanding the behavior in the nonlinear regime for which numerical analysis is necessary for a quantitative treatment of the governing partial differential equations. An open problem is the connection between microscopic and macroscopic descriptions. This, for example, may be established through the construction of a plasticity framework capable of describing deformation at macroscopic scales (e.g. shear bands, localized macroscopic strain zones) based on physical processes at microscopic scales (e.g. dislocation structures/patterns) and accounting also for microscopic features (e.g. dislocation line tension). In connection with this, reference is made to a more recent approach which rather than using scalar density measures without internal 'structure', the dislocation densities contain information regarding the direction of motion of the represented dislocations in terms of additional 'configurational' coordinates. In two-dimensional situations this can be done by introducing signed dislocation densities which determine the direction of motion on the slip plane with respect to the applied stress (e.g. Groma, Csikor, & Zaiser, 2003), in analogy to the distinction between positive and negative dislocation densities first introduced effectively in the W-A model (e.g. Walgraef & Aifantis, 1985b). In three-dimensional plasticity, on the other hand, it is in general necessary to endow the continuum theory with additional structure. This structure can consist of an additional dislocation velocity field as used in Sedlacek, Schwarz, Kratochvil, and Werner (2007), provided that such a field can be defined without ambiguity (this requires that each material volume element contains only dislocations of a single orientation).

Another approach initiated in El-Azab (2000) and further pursued in Hochrainer, Zaiser, and Gumbsch (2007), Sandfeld, Hochrainer, Zaiser, and Gumbsch (2011) distinguishes dislocations according to their orientation, and thus operates in a higher-dimensional state space. In such an approach, additional information about dislocation curvature must be included to correctly describe the changes in line length (and thus dislocation density) associated with the expansion or contraction of curved dislocation segments during their motion. In such a higher-dimensional formulation, the concept of dislocation transport needs to be extended to the additional 'configurational' coordinates to account for changes in the direction and curvature of segments (Hochrainer et al., 2007; Sandfeld et al., 2011). Irrespectively of the details of the kinematics, non-local dislocation interactions can, because of the presence of screening correlations, be represented in terms of gradient expansions (Groma et al., 2003) which make the dislocation velocities depend in a non-local manner on the dislocation densities, as also discussed herein. From the viewpoint of dislocation density dynamics, this leads to diffusion-like terms in the equations of evolution as used in the original W-A model. Beyond this formal similarity, these more recent models allow to link the diffusion-like terms to the strain gradients used in phenomenological gradient plasticity, as oriented dislocation densities can be directly related to strain gradients. Thus, it may be argued that such dislocation-density based framework possesses the structure of a second-order gradient plasticity theory, and indeed produces results similar to those obtained by strain gradient plasticity when applied to the problem of microbending (Aifantis, Weygand, Motz, Nikitas, & Zaiser, 2012). [For another recent account of dislocation dynamics description of the microbending problem and polygonization, the reader is referred to Le and Nguyen (2010).] These current developments of dislocation density dynamics may thus pave the way towards a unification of two strands of development - gradient dislocation dynamics as starting from the original W-A model, and gradient plasticity – towards a comprehensive substructure-based theory of plastic flow.

References

Aifantis, E. C. (1984). On the microstructural origin of certain inelastic models. *Journal of Engineering Materials Technology, 106*, 326–330.
Aifantis, E. C. (1987). The physics of plastic deformation. *International Journal of Plasticity, 3*, 211–247.
Aifantis, E. C., Walgraef, D., & Zbib, H. M. (1988). Guest Editors, Material Instabilities, Special Issue of *Res Mechanica, Vol. 23*.

Aifantis, K. E., Motz Weygand, D., C. Nikitas, N., & Zaiser, M. (2012). Modeling microbending of thin films through discrete dislocation dynamics, continuum dislocation theory, and gradient plasticity. *Journal of Materials Research, 27*, 612–618.

Aifantis, K. E., & Willis, J. R. (2005). The role of interfaces in enhancing the yield strength of composites and polycrystals. *Journal of Mechanics and Physics Solids, 53*, 1047–1070 [see also: K.E. Aifantis W.A. Soer, J.Th.M. De Hosson and J.R. Willis, Interfaces within strain gradient plasticity: Theory and experiments, *Acta Mater*. 54, 5077–5085, 2006.].

Benson, D. L., Maini, P. K., & Sherratt, J. A. (1997). Unravelling the Turing bifurcation using spatially varying diffusion coefficients. *Journal of Mathematical Biology, 37*, 381–417.

Berdichevskii, V. L., & Sedov, L. I. (1967). Dynamic theory of continuously distributed dislocations. Its relation to plasticity theory. *Journal of Applied Mathematics and Mechanics (PMM), 31*, 981–1000.

Berdichevskii, V., & Truskinovskii, L. (1985). Energy structure of localization. In P. Lavedeze (Ed.), *Studies in applied mechanics 12: Local effects in the analysis of structures* (pp. 127–158). Elsevier.

Berdichevsky, V. L. (2008). Entropy of microstructure. *Journal of the Mechanics and Physics of Solids, 56*, 742–771 [see also: V.L. Berdichevsky, Structure of equations of macrophysics Phys. Rev. E 68 066126/1-26, 2003.].

Berdichevsky, V. L. (2009). *Variational principles of continuum mechanics* [Vols. I(Fundamentals) & II (Applications)]. Springer.

Calisto, H., Clerc, M., Rojas, R., & Tirapegui, E. (2000). Bubbles interactions in the Cahn–Hilliard equation. *Physical Review Letters, 85*, 3805–3808.

Dee, G. T., & van Sarloos, W. (1988). Bistable system with propagating fronts heading to pattern formations. *Physics Review Letters, 60*, 2641–2644 [see also: W. van Sarloos. (1989). Front propagation into unstable states-II: Linear versus nonlinear marginal stability and rate convergence, *Phys. Rev. A39*, 6367–6390.].

El-Azab, A. (2000). Statistical mechanics treatment of the evolution of dislocation distributions in single crystals. *Physical Review B, 61*, 11956–11966.

Essmann, U., & Mughrabi, H. (1979). Annihilation of dislocations during tensile and cyclic deformation and limits of dislocation densities. *Philosophical Magazine A, 40*, 731–756 [see also: P. Neumann, The interactions between dislocations and dislocation dipoles, *Acta Met.* 19, 1233–1241, 1971.].

Fleck, N. A., Muller, G. M., Ashby, M. F., & Hutchinson, J. W. (1994). Strain gradient plasticity: Theory and experiment. *Acta Metallurgica Materialia, 42*, 475–487 [see also: N.A. Fleck and J.W. Hutchinson, A reformulation of strain gradient plasticity, J. Mech. Phy. Solids 49, 2245–2272, 2001.].

Ghoniem, N. M., Busso, E., Kioussis, N., & Huang, H. (2003). Multiscale modeling of nano and micro mechanics: An Overview. *Philosophical Magazine A, 83*, 3475–3528.

Gregor, V., & Kratochvil, J. (1998). Self-organization approach to cyclic microplasticity: A model of a persistent slip band. *International Journal of Plasticity, 14*, 159–172 [see also: M. Saxlova, J. Kratochvil, J. Zatloukal, The model of formation and disintegration of vein dislocation structure, *Mat. Sci. Engng.* A, 234–236, 205–208, 1997; J. Kratochvil and M. Saxlova, Sweeping mechanism of dislocation pattern formation, *Scripta Metall. Mater.* 26, 113–116, 1992.].

Groma, I. (1997). Link between the microscopic and mesoscopic length-scale description of the collective behavior of dislocations. *Physical Review B, 56*, 5807–5813.

Groma, I., Csikor, F., & Zaiser, M. (2003). Spatial correlations and higher-order gradient terms in a continuum description of dislocation dynamics. *Acta Materialia, 51*, 1271–1281.

Gurtin, M. E., & Anand, L. (2009). Thermodynamics applied to gradient theories involving the accumulated plastic strain. The theories of Aifantis & Fleck and Hutchinson and their generalization. *Journal of the Mechanics and Physics of Solids, 57*, 405–421 [see also: S. Forest and E.C. Aifantis, Some links between recent gradient thermo-elasto-plasticity theories and the thermodynamics of generalized continua, *Int. J. Solids Struct.*, 47, 3367–3376, 2010; E.C. Aifantis, Update on a class of gradient theories, *Mech. Mater.*, 35, 259–280, 2003; E.C. Aifantis, On scale invariance in anisotropic plasticity, gradient plasticity and gradient elasticity, *Int. J. Engng. Sci.*, 47, 1089–1099, 2009.].

Hochrainer, T., Zaiser, M., & Gumbsch, P. (2007). A three-dimensional continuum theory of dislocation systems: Kinematics and mean field formulation. *Philosophical Magazine, 87*, 1261–1282.

Huang, H., Ghoniem, N., de la Rubia, T. D., Ree, M., Zbib, H. M., & Hirth, J. P. (1999). Stability of dislocation short-range reactions in bcc crystals. *Journal of Engineering Materials and Technology, 121*, 143–150.

Kubin, L. P. (1993). Dislocation patterning. In: Treatise on Materials Science and Technology, Cahn, R. W., Haasen, P., Kramer, E. J. Vol. 6, Chapter 4, VCH Weinberg (pp. 137–190).

Le, K. C., & Nguyen, Q. S. (2010). Polygonization as low energy dislocation structure. *Continua Mechanics and Thermodynamics, 22*, 291–298 [see also: K.C. Le and B.D. Nguyen, Polygonization: Theory and comparison with experiments, preprint, 2011.].

Needleman, A. (1990). An analysis of decohesion along an imperfect interface. *International Journal of Fracture, 42*, 21–40.

Pontes, J., Walgraef, D., & Aifantis, E. C. (2006). On dislocation patterning: Multiple slip effects in the rate equation approach. *International Journal of Plasticity, 22*, 1486–1505.

Rhee, M., Zbib, H. M., Hirth, J. P., Huang, H., & de la Rubia, T. D. (1998). Models for long-/short-range interactions and cross slip in 3D dislocation simulation of BCC single crystals. *Modelling and Simulation Material Science Engineering, 6*, 467–492.

Sandfeld, S., Hochrainer, T., Zaiser, M., & Gumbsch, P. (2011). Continuum modeling of dislocation plasticity: Theory, numerical implementation and validation by discrete dislocation simulations. *Journal of Materials Research, 26*, 623–632.

San Miguel, M., Montagne, R., Amengual, A., & Hernandez, G. (1996). In E. Tirapegui & W. Zeller (Eds.), *Instabilities and Nonequilibrium Structures V* (pp. 85–97). Dordrecht: Kluwer.

Sedlacek, R., Schwarz, C., Kratochvil, J., & Werner, E. (2007). Continuum theory of evolving dislocation fields. *Philosophical Magazine A, 87*, 1225–1260.

Shi, Q. (2004). *Finite element analysis of strain gradient plasticity in strain softening materials. Computational mechanics WCCM VI in conjunction with APCOM'04*. Beijing, China: Tsinghua University Press & Springer-Verlag, pp. 5–10 [see also: Q. Shi, C.S. Chang, Numerical Analysis for the effect of heterogeneity on shear band formation, 16thASCE Eng. Mech. Conference, July 16th–18th (2003), University of Washington, Seattle.].

Tabata, T., Fujita, H., Hiraoka, M., & Onishi, K. (1983). Dislocation behavior and the formation of persistent slip bands in fatigued copper single crystals observed by high-voltage electron microscopy. *Philosophical Magazine A, 47*, 841–857.

Vardoulakis, I., & Aifantis, E. C. (1989). Gradient dependent dilatancy and its implications in shear banding and liquefaction. *Ing Archives, 59*, 197–208 [see also: Peerlings, R.H.J., de Borst, R., Brekelmans, W.A.M. de Vree, J.H.P. (1996). Gradient-enhanced damage for quasi-brittle materials, *International Journal of Numerical Methods in Engineering, 39*, 3391–3403.].

Walgraef, D. (1996). *Spatio–Temporal pattern formation (with examples in physics, chemistry and materials science)*. New York: Springer-Verlag.

Walgraef, D. (2002). Rate equation approach to dislocation dynamics and plastic deformation. *Materials Science & Engineering A, 322*, 167–175.

Walgraef, D. (2003). Nanostructure evolution during thin film deposition. *Physica E, 18*, 393–401.

Walgraef, D. (2003). Reaction–diffusion approach to nanostructure formation during thin film deposition. *Philosophical Magazine A, 83*, 3829–3846.

Walgraef, D., & Aifantis, E. C. (1985a). On the formation and stability of dislocation patterns -I, -II, -III. *International Journal of Engineering Science, 23*, 1351–1358.

Walgraef, D., & Aifantis, E. C. (1985b). Dislocation patterning in fatigued metals as a result of dynamical Instabilities. *Journal of Applied Physics, 58*, 688–691 [see also: Walgraef, D. & Aifantis, E. C. (1988). Plastic instabilities, dislocation patterns and nonequilibrium phenomena, *Res Mechanica, 23*, 161–195.].

Walgraef, D., & Aifantis, E. C. (2009). On dislocation patterning: Revisiting the W–A model: Part I–The role of stochastic terms in dislocation dynamics; Part II–The role of stochastic terms in dislocation dynamics. *Journal of Mechanical Behaviour of Materials, 19*(49-65), 67–82 [see also: D. Walgraef and E.C. Aifantis, On the gradient theory of elasticity and dislocation dynamics, in: A. El-Azab (ed.) Proc. 4th Int. Conference on Multiscale Materials Modeling/ MMM2008, Dept. Scient. Comput., Florida State University, pp. 720–725, 2008.].

Walgraef, D., Ghoniem, N., & Lauzeral, J. (1997). Deformation patterns in thin films under uniform laser irradiation. *Physical Review B, 56*, 15361–15377.

Zaiser, M., Miguel, M., & Groma, I. (2001). Statistical dynamics of dislocation systems: The influence of dislocation–dislocation correlations. *Physical Review B, 64*(224102), 1–9 [see also: Zaiser, M. (2001). Statistical Modeling of dislocation systems, *Materials Science & Engineering A*, 309–310, 304–315.].

Zbib, H. M., & Aifantis, E. C. (1988). On the localization and post localization behavior of plastic deformation-I.,II,III. *Res Mechanica, 23*, 261–305.